Spectrochimica Acta Part A: Molecular and Biomolecular Spectroscopy 275 (2022) 121153

Contents lists available at ScienceDirect

Spectrochimica Acta Part A: Molecular and Biomolecular Spectroscopy

journal homepage: www.elsevier.com/locate/saa

A Fourier-domain-based line shape recovery method used in direct absorption spectroscopy

Rui Liang [a], Fupeng Wang [a,b,*], Qingsheng Xue [a], Qiang Wang [b], Jinghua Wu [a], Yaopeng Cheng [a], Qian Li [a]

[a] College of Information Science and Engineering, Ocean University of China, Qingdao, China
[b] State Key Laboratory of Applied Optics, Changchun Institute of Optics, Fine Mechanics and Physics, Chinese Academy of Sciences Changchun, 130033, China

HIGHLIGHTS

- The first Fourier-domain-based absorption profile recovery method;
- Self-calibration function to eliminate influence of optical power fluctuation;
- Ultra-easy implementation based on software or hardware platform.

GRAPHICAL ABSTRACT

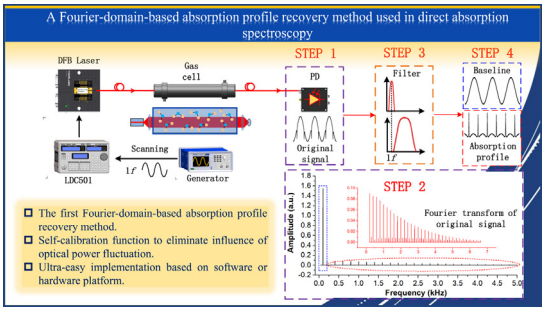

ARTICLE INFO

Article history:
Received 7 December 2021
Received in revised form 7 March 2022
Accepted 11 March 2022
Available online 14 March 2022

Keywords:
Sinewave scanning
Fourier domain
Line shape recovery
Self-calibration
Direct absorption spectroscopy

ABSTRACT

A novel absorption line shape recovery method with self-calibration function and ultra-easy implementation was introduced to direct absorption spectroscopy (DAS) in this study. The self-calibration function empowered the DAS system with the immunity to the laser power fluctuations. The ultra-easy implementation was achieved in that the DAS system was substantially simplified with a single-path DAS rather than the traditional dual-path differential optical absorption spectroscopy (DOAS), and the absorption profile can be directly recovered by an analog or digital filter instead of complex fitting algorithm or sophisticated balance detection circuits. The reliability and self-calibration characteristic of the new method were validated using CH_4 transition at 1653.72 nm, where the line strength is 1.45×10^{-21} cm/molec. The Voigt fitting residual and signal to noise ratio were optimized in detail and compared with the DOAS.

1. Introduction

Trace gas detection is of great interest in a wide range of applications, such as food & medicine safety, combustion analysis, environmental monitoring and industrial process control [1–5]. Among large number of technologies, tunable diode laser absorption spectroscopy (TDLAS) has become the preferred opinion due to its inherent advantages such as excellent selectivity, high sensitivity, robust anti-interference ability and long service life. In the TDLAS-based systems, the direct absorption spectroscopy (DAS) has the simplest system diagram. To improve the detection sensitivity of TDLAS system, mid-infrared (MIR) lasers were preferred to exploit the strong fundamental rotation/vibration absorption lines [6–8], because the absorption line strength of gas molecule in the MIR region is, generally, three orders of magnitude higher than the near infrared (NIR) band. Recently, the rapid development of MIR tunable light source, such as inter-band cascade laser (ICL), quantum cascade laser (QCL), further reduced the cost and complexity of the MIR light source based TDLAS system compared to

* Corresponding author.
E-mail address: wfp@ouc.edu.cn (F. Wang).

https://doi.org/10.1016/j.saa.2022.121153
1386-1425/

the past [9–13]. However, the need to actively cool both the lasers and detectors restricted the widespread use of such MIR systems. So, in order to secure the high detection sensitivity, the wavelength modulation spectroscopy (WMS) was proposed later and immediately drawn many attentions owing to its excellent noise rejection performance by virtue of the harmonic detection technology [14 15]. In addition to the above mentioned direct absorption technology, several indirect absorption spectroscopy (IDAS) techniques were successively proposed and attracted many attentions such as photoacoustic spectroscopy (PAS) [16 17], photothermal spectroscopy (PTAS) [18] and light-induced thermoelastic spectroscopy (LITES) [19 20]. These IDAS techniques all have a specific characteristic of background free. Furthermore, they have the ability to bring the trace gas detection to ultra-high sensitivity, and minimum detection limit (MDL) of parts per trillion level has been achieved in published studies. Though the WMS technique and recently developed IDAS dominated with the advantage of high signal to noise ratio (SNR), however the DAS is still indispensable in many situations because of its capability of directly measuring the absorption profiles. There, efforts are still needed to paid to improve the performance of DAS systems.

In the DAS system, the most critical procedure is to recover the absorbance curve from the transmitted light signal I_t. According to the Beer-Lambert law $I_t = I_0 \cdot e^{-\alpha cL} \approx I_0 \cdot (1 - \alpha cL)$, the incident light intensity (baseline) I_0 should be measured in advance. To achieve the above processing, there are two mainstream approaches. One is called differential optical absorption spectroscopy (DOAS), in which the light source is split into reference arm and sensing arm by a 1×2 coupler. As a result, the baseline I_0 and transmitted signal I_t can be easily detected. Afterwards, the absorbance profile is obtained by a balanced photo-detector. In another method, a polynomial fitting is applied to the non-absorbed portion of the transmitted signal I_t to simulate the baseline I_0. Then the absorbance profile can be calculated as well. To our knowledge and experience on TDLAS applications, there are several problems in the above methods. (i) The DOAS structure is beneficial to suppress the common mode interference, however it is very sensitive to the optical power fluctuations. A minor drift of light source would break the balance of the differential circuit, resulting in distortion of demodulated absorbance curve. The polynomial fitting method also suffered from the effect of optical power fluctuations. In addition, the common mode noise suppression does not work in the fitting process. In some harsh application conditions, the high noise level perhaps bring in additional fitting error. (ii) Triangular or sawtooth wave is usually employed to scan the laser wavelength. However, the frequency components of triangular or sawtooth wave are so complex that the circuits should have a large measuring bandwidth to be compatible. This limits the scanning frequency in the range lower than 10 kHz [21], which decreases the time resolution. Furthermore, the steep changes in triangular and sawtooth wave could affect the working stability of laser source according to our published study [22]. (iii) The ground-truth baseline I_0 is not easy to achieve because of the finite scanning width and line broadening. Moreover, the nonlinearity of wavelength and power response towards the driving current would make troubles in baseline determining and absorption calculating.

Efforts have been made to solve the mentioned problems. In DOAS system, the reference arm can be used to monitor the laser power fluctuations in addition to calculating the incident light I_0. The power drift was normalized at the cost of further complicating the DOAS system. In addition, the non-homologous normalization may introduce unexpected correction errors due to the differential mode interference between sensing arm and monitoring arm. In 2015, we proposed a “head–tail” demodulation algorithm based merely on the sensing arm to successfully recover the absorption profile, which was verified immune to light power drift [23]. Recently, Prof. Peng et al. introduced a high-accuracy sinewave-scanned DAS technique, in which a fitting routine was developed based on the explicit baseline expression and accurate wavelength calibration [24]. With this method, the incident light intensity and the absorbance profile can be synchronously obtained by fitting the transmitted light in time domain. To further simplify the system structure and carry forward the working mode of sinewave-scanned DAS, we reported a Fourier-domain-based absorption line shape recovery method in this paper. Compared with triangular or sawtooth wave, sinewave has very clear frequency component. So, the sinewave scanned baseline can be separated from the absorption information in the Fourier spectrum easily. Afterwards, we applied two filters to detect the incident light information I_0 and absorption profile from transmitted signal I_t, and the absorption profile was normalized by the separated I_0 to eliminate the influence of laser power fluctuations. In this method, the signal I_0 used for normalization was totally homologous with recovered absorption profile.

The rest of this study was organized as follows. Section 2 introduced the fundamentals of the Fourier-domain-based line shape recovery method (FD-DAS). Section 3 demonstrated the experiment system and how the experiment conducted. Section 4 presented the experimental results and provided a brief comparison with DOAS. Section 5 discussed the advantages and limitations of the FD-DAS method. Finally, Section 6 concluded this study.

2. Methodology

Temporarily limited by our experimental conditions, the nonlinear effect of laser output is ignored in our study. The influence of laser nonlinearity on the FD-DAS will be analyzed in the discussion section. So, when we use sinewave current to drive the laser source, its intensity and wavelength output can be described as,

$$I_0(t) = \bar{I} + i\cos(2\pi ft) \tag{1}$$

$$v(t) = v_0 + \delta\cos(2\pi ft + \varphi') \tag{2}$$

where $\bar{I}$ is the laser output average intensity, i is the intensity scanning depth, f is the scanning frequency, v_0 is the average wavelength which is expected to be located at the center of absorption line shape, δ is the wavelength scanning depth and φ' is the phase difference between the wavelength and intensity response. When the output light passes through the sample gas, the transmitted light is detected by a photodetector as,

$$I_t(t) = I_0(t) \cdot exp[-\alpha(v)cL] \tag{3}$$

where $\alpha(v)$ is the absorption coefficient, which is a function of wavelength v, c is the concentration of sample gas at unit of ppm, L is the length of absorption path. Considering the analogy between the above equations and the Eq. (3), 4 in WMS method [25], it is equivalent to fixing the wavelength at a constant v_0 and applying a large modulation depth δ to modulate the absorption profile. When performing the harmonic analysis, the detected signal $I_t(t)$ in Eq. (3) can be divided as:

$$I_t(t) = \{\underbrace{(V_{DC} \propto \bar{I})}_{p^1} + \underbrace{(V_{indep_{1f}} \propto i)}_{p^2} + \underbrace{[(V_{dep_{1f}} + V_{dep_{2f}} + V_{dep_{3f}} + V_{dep_{4f}} + \cdots) \propto (\alpha cL)]}_{p^3}\} \tag{4}$$

where V_{DC} represents the DC signal depending on the average intensity $\bar{I}$, $V_{indep_{1f}}$ is the absorption independent 1f component which is related to the intensity scanning depth i, the item p_3 includes all the absorption dependent harmonic signals. Only

considering pure wavelength modulation in WMS system, the odd harmonics are centrosymmetric about the center of absorption profile and the even harmonics are symmetric. As a result, the amplitudes of odd harmonics $V_{dep_{1f}}$, $V_{dep_{3f}}$, $V_{dep_{5f}}$ ... should be zero while the even harmonics $V_{dep_{2f}}$, $V_{dep_{4f}}$, $V_{dep_{6f}}$ ... reach their maximum value if we fix the v_0 at the absorption center precisely.

In addition to the above analysis, experimental results plot here in Fig. 1 helps to understand how the FD-DAS works. A 100 Hz (1f) sinewave current is used to drive the laser source, the transmitted light is detected as shown in Fig. 1 (a), the absorption curves appear at the rising and falling edge of sinewave signal. To get a highly authentic Fourier spectrum as shown in Fig. 1 (b), 128 cycles of such sinewave signal in Fig. 1 (a) are saved to do the Fourier transform in our study. The absorption independent 1f component is marked with a dashed box in its Fourier spectrum as shown in Fig. 1 (b), which can be separated using a narrow bandpass filter as shown in Fig. 1 (c). The Fourier spectrum of absorption dependent harmonics is circled by a dotted oval as shown in Fig. 1 (b). To obtain the absorption profile in time domain from the Fourier spectrum, we can apply a $> 1f$ high-pass or bandpass filter to the original signal in Fig. 1 (a). The corresponding absorption profile signal is recovered as shown in Fig. 1 (d). In the next step of our FD-DAS technique, the recovered absorption profile in Fig. 1 (d) can be used to calculate the absorption-related parameters such as gas concentration, temperature, pressure, etc. The extracted baseline in Fig. 1 (c) represents the power stability of the laser output, which can be used to counteract influence of laser power fluctuations. We have to clarify that large 0 Hz component should be observed in Fig. 1 (b) due to the DC offset involved in the detected signal as shown in Fig. 1 (a). In order to make the 1f component and absorption dependent harmonics more observable in Fourier spectrum, the large 0 Hz spectrum peak is cut off from the Fig. 1 (b) Fourier spectrum for better display.

3. Experimental setup

A schematic of experimental system is depicted in Fig. 2. To verify the FD-DAS method, the CH_4 is chosen as the object gas. The CH_4 has a strong absorption at 1653.72 nm (6046.97 cm^{-1}), where the intensity of absorption line is $1.45 \times 10^{-21} cm^{-1}/(mol \cdot cm^{-2})$ according to HITRAN 2016. Hence, a DFB laser operated at 1653 nm is utilized as the light source in this system. The DFB laser is controlled and driven by the LDC501 (Stanford Research System, USA), operating at a temperature of 30.9 °C. The wavelength scanning is realized by a 100 Hz sinewave (p-p 0–3 V) generated by a generator (AFG1000, Tektronix, USA). The laser output propagates to a fiber coupled Herriott cell (3 m path-length) to interact with CH_4 molecules, and the transmitted light signal is measured by a photodetector for photoelectric conversion to get the original signal as shown in Fig. 2. Then, two filters are applied to the original signal to separate the sinewave baseline and absorption information. The center frequency of the first filter is located at 100 Hz ($1f$) and its bandwidth is compressed sharply to 10 Hz. The parameters of another filter would be optimized in Section 4 for a best absorption profile recovery. Amplitude of the separated sinewave baseline is used to calibrate the absorption signal to eliminate the influence of laser power fluctuations, realizing the self-calibration function. The sample gas used in this experiment is provided by a gas mixing system as shown in Fig. 2, including a customized mixing chamber, two flowmeters, 99.999% pure nitrogen and 1% methane.

4. Experimental results

4.1. Absorption profile recovery

To evaluate the performance on absorption profile recovery of FD-DAS method, the Voigt profile was used to fit the measured absorption signal, and compared it with the results from DOAS method as shown in Fig. 3. All the data were acquired in the same photoelectric detection condition to guarantee the accuracy of comparison.

As mentioned in section 2, a high-pass filter ($> 1f$) is the best choice to recover the absorption profile since all the absorption dependent harmonics are included in the passband, leading to no absorption information loss in the filtering process. However, some

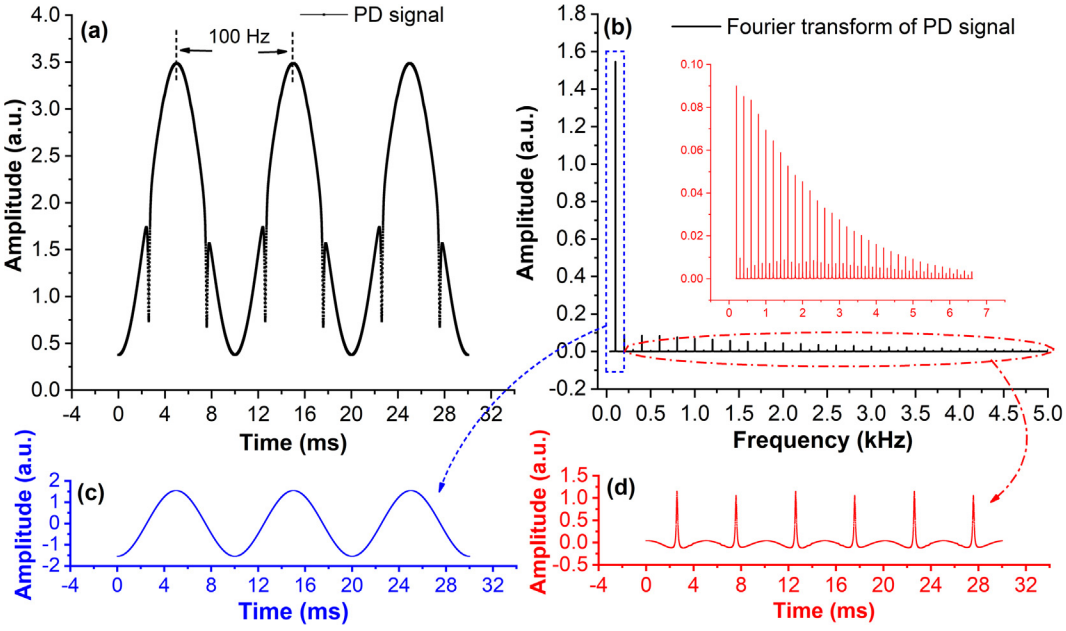

Fig. 1. The principle of the FD-DAS method. (a) the detected transmitted light signal I_t, (b) the Fourier spectrum of transmitted light signal, (c) the sinewave scanning baseline extracted from I_t, (d) the recovered absorption profile signal extracted from I_t.

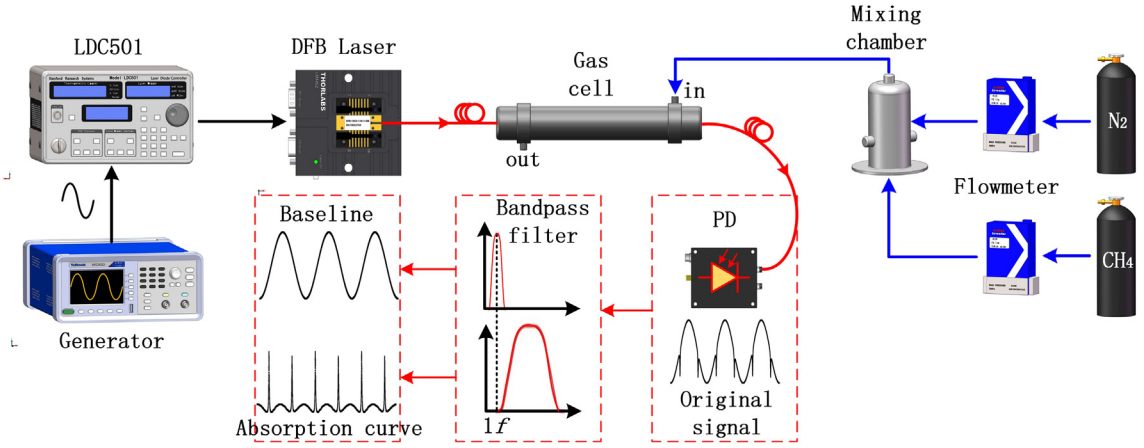

Fig. 2. The schematic of FD-DAS experimental system.

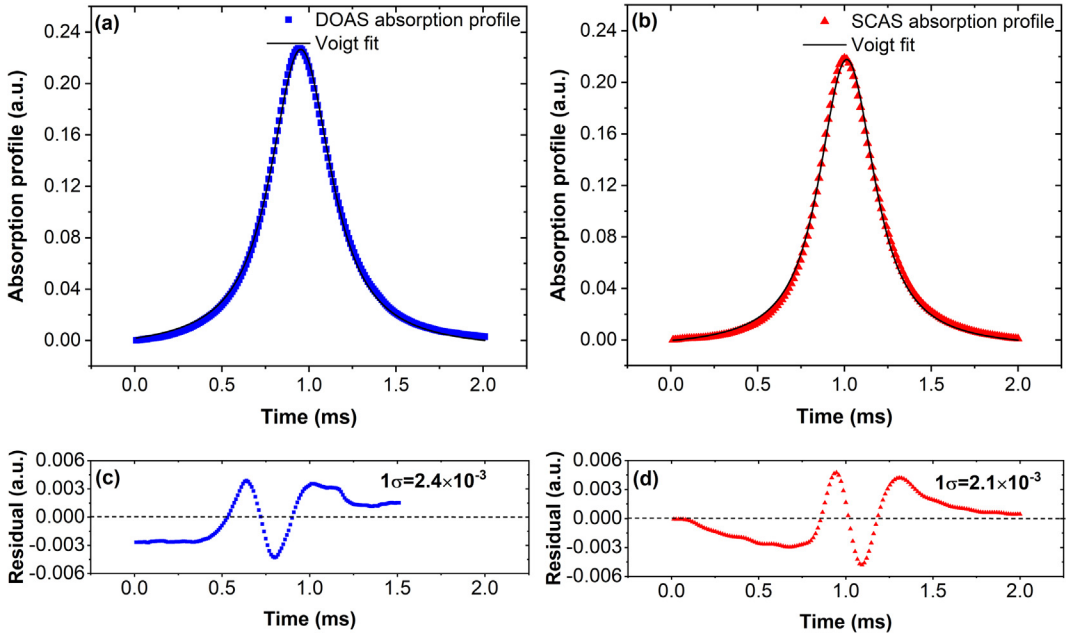

Fig. 3. The Voigt fitting and residual analysis of demodulated absorption profiles.

harmonics may appear from the absorption independent baseline due to the nonlinearity effect and noises also distribute in some frequency band. Therefore, we applied a bandpass filter to get the absorption profile in our method in the very beginning. So, the low-frequency edge (f_L) and high-frequency edge (f_H) were optimized in experiments to improve performance. The results are displayed in Fig. 4.

Firstly, we increased the f_L by the step of 10 Hz from 100 Hz to 800 Hz, the Voigt fitting was performed at each situation and the corresponding residual was calculated such as Fig. 3 (b) and (d). The standard deviation of each residual was plotted in the function of f_L in Fig. 4 (a). We observed that the residual improved first and then deteriorated as the f_L increasing, as a result, frequency of 300 Hz was the optimal choice of f_L. If the f_L is lower than 300 Hz, the harmonics from p_2 nonlinearity would disturb the recovered absorption profile. If the f_L was set too high, then much absorption information would be eliminated, worsening the Voigt fitting results. So, the f_L of bandpass filter was set to 300 Hz. Secondly, we used the same strategy to optimize the f_H as plotted in Fig. 4 (b). The Fig. 4(b) told us most of the effective absorption information was limited within 10 kHz. As a conclusion of this part, we set the bandpass filter from 300 Hz to 10 kHz to extract the absorption profile. The Voigt fitting was performed and residual was calculated as demonstrated in Fig. 3 (b) and (d), reaching a comparable level compared with the DOAS method as shown in Fig. 3 (a) and (c). Considering the obvious add/even characteristic in Fig. 3 (d), we applied our published "head–tail" algorithm to further process the filtered absorption profile. Finally, the standard deviation of residual was improved to 3.6×10^{-4} as shown in Fig. 5, which was way better than DOAS results.

4.2. Signal to noise ratio

Considering that filtering process was used as the fundamental technique in FD-DAS, we expected it should have advantages on SNR improvement over DOAS method. By the way, SNR was used to optimize the f_L and f_H of bandpass filter. Absorption amplitude was defined as shown in Fig. 9 (a), and standard deviation of non-absorption baseline was calculated as the noise, as a result the SNR

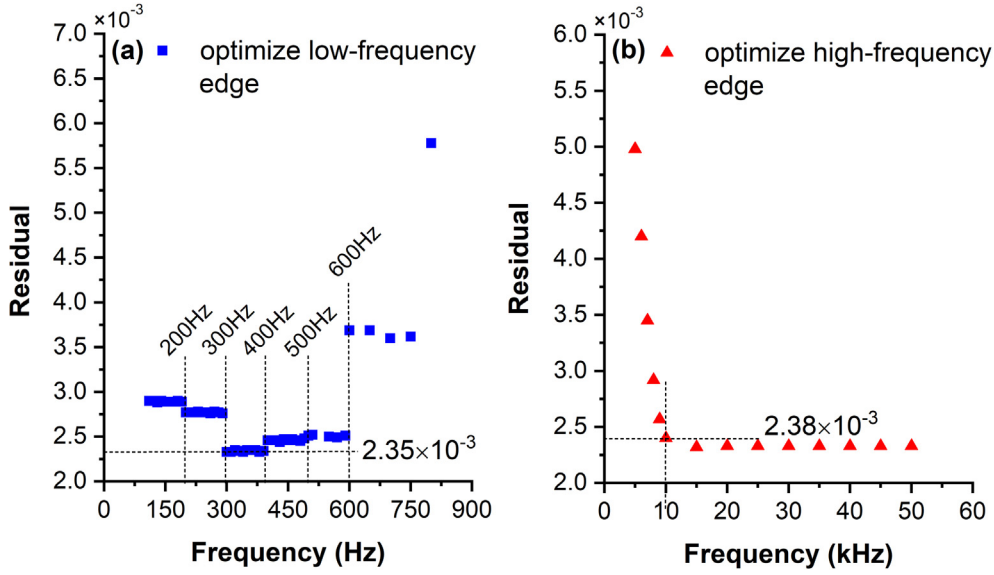

Fig. 4. Optimization of filtering frequency of bandpass filter. (a) the low-frequency edge of bandpass filter affects the residual of Voigt fitting, (b) the high-frequency edge of bandpass filter affects the residual of Voigt fitting.

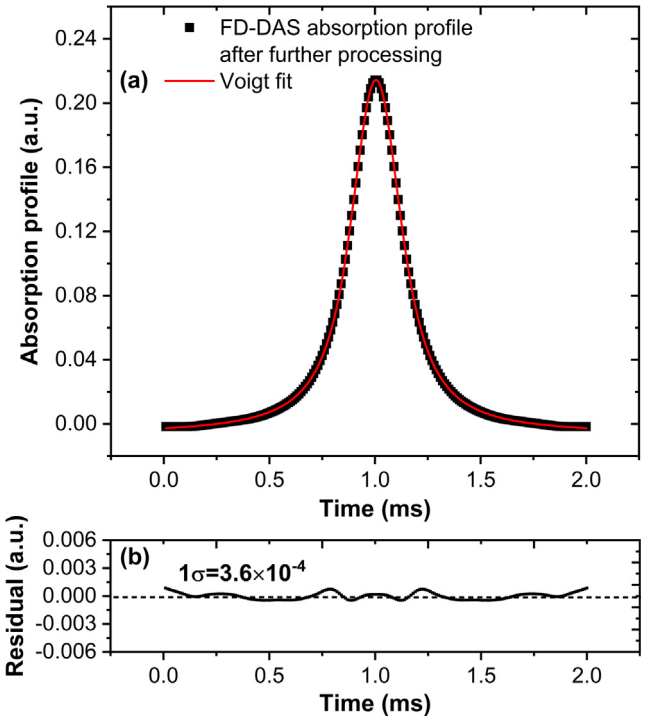

Fig. 5. The Voigt fitting and residual results after applying "head–tail" algorithm.

was defined by dividing absorption amplitude with the calculated noise in this section. In the similar way discussed in the Section 4.1, the f_L was increased by the step of 10 Hz from 100 Hz to 800 Hz to determine the low-frequency edge firstly, and secondly the f_H was optimized by increasing it from 5 kHz to 60 kHz as shown in Fig. 6.

The SNR was calculated to be 641 in the same way based on the DOAS method, which was marked with a chain line as shown in Fig. 6 for comparison. The best SNR appeared at frequency of ~ 300 Hz when optimizing the f_L and then decreased rapidly because of the loss of the primary absorption dependent even harmonics. Afterwards, the optimal high frequency edge was verified by comparing the SNR in different f_H values from 5 kHz to 50 kHz. The SNR improved gradually at the beginning mainly because the absorption amplitude increased due to including more higher harmonics within the passband. Further increasing the f_H, the SNR almost did not change. We analyzed the reasons as: (i) Although more and more absorption dependent harmonics are included as we increased the frequency edge f_H, however, their contribution to the absorption amplitude is very little. As a result, the measured absorption amplitude almost does not increase any more. (ii) Noises distribute at high frequency range are very low duo to the $1/f$ noise characteristic. As a result, the bandwidth of bandpass filter was set from 300 Hz to 12 kHz. A SNR of 880 was achieved which was better than 641 of DOAS.

To sum up the Section 4.1 and 4.2, the bandwidth should be set as 300 Hz ~ 12 kHz combining the results of Fig. 4 and Fig. 6 if we use a bandpass filter to realize the absorption profile recovery as we thought in the very beginning. Of course, we can also simply use a highpass filter instead because the high frequency edge f_H seems not to affect the results of both Voigt fitting and SNR in environment without high-frequency noise. Cliffs were observed at 200 Hz, 300 Hz, 400 Hz, 500 Hz in Fig. 4 (a) and Fig. 6 (b) because of including or excluding the relative absorption dependent harmonics.

4.3. Self-calibration characteristic of FD-DAS compared with conventional DOAS

The technical process of self-calibration function is as follows: A bandwidth of 10 Hz bandpass filter centered at 100 Hz was applied to the detected original signal as displayed in Fig. 1 (a), then the sinewave scanning baseline was extracted. It's easy to understand that the sinewave amplitude represents the laser output power level. Thus, it can be used to calibrate the fluctuation influence of light source itself. However, the above filtering process and preamp circuits should be stable and accurate to guarantee the reliability of self-calibration function. Therefore, we performed a brief experiment to validate the stability and accuracy in advance. When the sinewave baseline was extracted, its amplitude (p-p value) was calculated and recorded in Fig. 7, compared to an average amplitude of 3.0956 V, a standard deviation of 5.2×10^{-5} was achieved which indicated the stability of both bandpass filter and our preamp circuits was good enough to calibrate the light power fluctu-

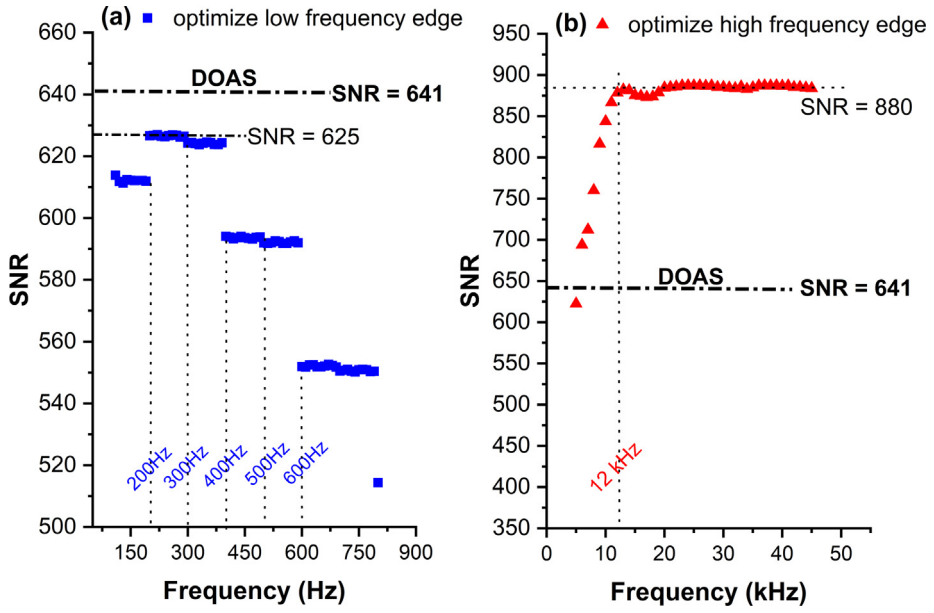

Fig. 6. Using SNR to optimize the filtering frequency of bandpass filter. (a) the low-frequency edge of bandpass filter affects the SNR of absorption signal, (b) the high-frequency edge of bandpass filter affects the SNR of absorption signal.

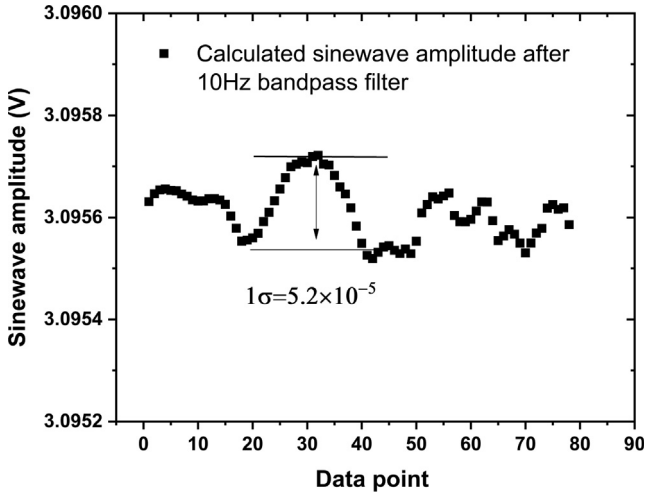

Fig. 7. Preliminary verification of the stability and accuracy of the sinewave baseline extraction.

ations. As to the accuracy, the sinewave p-p amplitude declined to 3.0956 V from actual ~ 3.1 V of original signal. The minor drop ~ 5 mV comes from the filtering loss, which is reasonable.

Since the filtering process is reliable, experiment system was modified as shown in Fig. 8 to validate the self-calibration function towards laser power fluctuations, and compared to the DOAS method. Artificial optical attenuations were introduced to position A and B by modulating the fiber attenuator respectively. Except for the difference between DOAS and FD-DAS absorption profile recovery method, the other experimental conditions were kept the same when performing the validation and comparison.

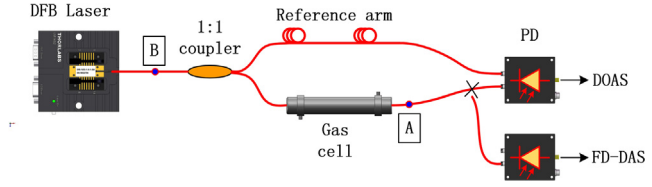

Fig. 8. Experimental diagram to verify the self-calibration characteristic of FD-DAS compared with conventional DOAS.

In the beginning, the DOAS structure was realized as shown in Fig. 8, and the differential circuit was adjusted to a balance state. It means that the voltage signals from reference arm and gas cell arm are approximately equal, as a result the baseline of demodulated absorption profile is flat in the non-absorption area. However, when extra attenuation was introduced at point A, the adjusted balance state was suddenly broken, thus an obvious distortion was observed in Fig. 9 (a) as depicted with blue triangular dots. When extra attenuation was introduced at common point B, the baseline of absorption profile biased as well as depicted with red circular dots in Fig. 9 (a). The reason was that the splitting ratio of the used 1:1 fiber coupler was not strictly 1:1 so that the power fluctuation at point B can still cause imbalance in DOAS method. In addition to that the optical attenuation occurred during light propagation can easily distort the demodulated absorption signal in DOAS method, the absorption amplitude (defined as Fig. 9a) in profile center would be cut down as well due to the decreased I_0 of detected voltage. So the absorption amplitude from DOAS method decreased as increasing the attenuation index at point A and B, resulting in a large amplitude difference compared to the FD-DAS method as shown in Fig. 9 (b). However, no obvious waveform distortion were observed in FD-DAS method whether modulating A or B. In a nutshell, the laser power fluctuations almost have no effect on the absorption amplitudes of FD-DAS.

5. Discussion

The proposed FD-DAS provides an absorption profile recovery method by filtering process in frequency domain for the first time. As analyzed in Section 2, the useful signals distribute at fundamental frequency of wavelength scanning and its harmonics. Theoretically, we can extract the exact characteristic frequency to recover the corresponding time-domain signal, and noise located at other frequencies can be eliminated effectively. For example, the $1f$ can be used to recover the scanning baseline and the $2f, 4f, 6f \cdots$ har-

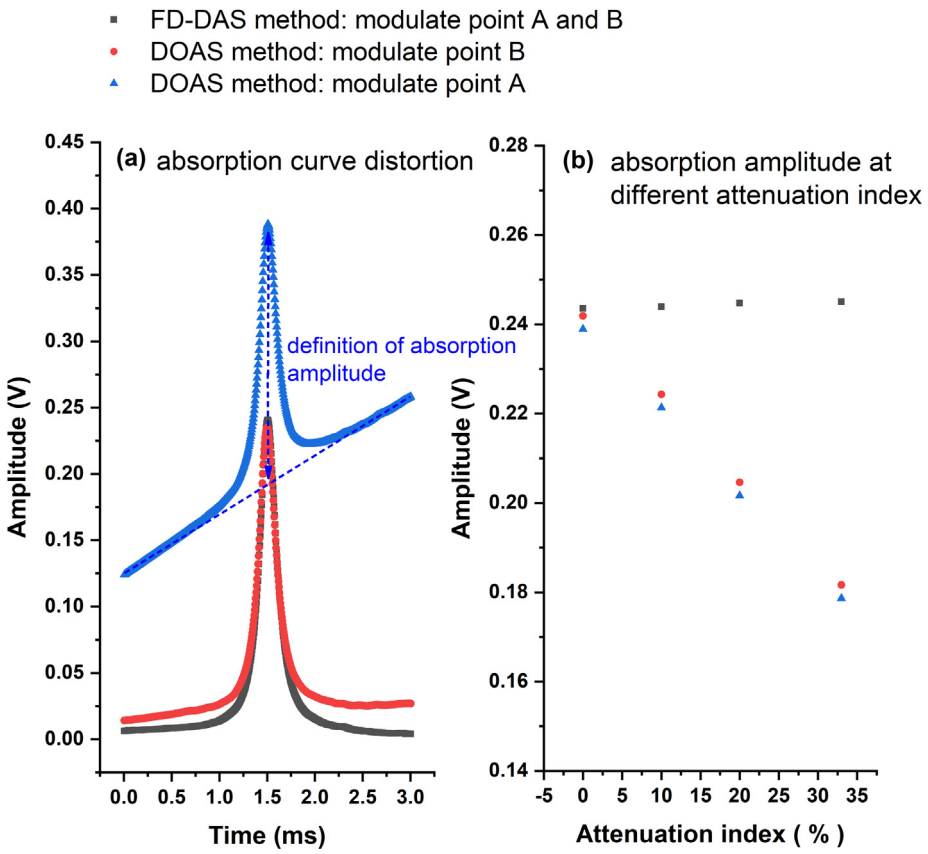

Fig. 9. Capability of calibrating the laser power fluctuations in FD-DAS and DOAS method. (a) the measured absorption signals in FD-DAS and DOAS methods when laser power attenuations introduced to light transmission. (b) the calculated absorption amplitudes in FD-DAS and DOAS methods towards different attenuation indexes.

monics can be chosen to recover the absorption profile. However, it is very complex to extract the characteristic frequency one by one to reconstruct the time-domain signal. Such a strategy can only be carried out by software post-processing and is time consuming. Hardware circuits are impotent to separate such a lot of discrete characteristic frequencies. Therefore, we use filtering process instead of characteristic frequency extraction in FD-DAS method, which is easier to implement because the filter can be realized by software or hardware circuits. Even the FD-DAS in this study is implemented based on software filter to demonstrate our idea for convenience. However, it can be realized by hardware or software depending on specific applications. If the resources for AD-collection and data processing are sufficient, we think all-software-based filtering and calculating is a good idea to simplify the gas detection system. If the computing resources are limited, hardware-based filtering and dividing circuits can be involved to share the workload. Furthermore, because we use sinewave to scan the laser instead of triangular or sawtooth wave in FD-DAS, it has capability to operate at a higher frequency . > 10 kHz to avoid the $1/f$ noise. Moreover, filter bandwidth can be optimized as we did in Section 4.1 and 4.2 to further improve the noise level. Another advantage of the FD-DAS is self-calibration to laser power fluctuations. The filtered baseline and absorption profile are homologous all the time, ensuring the reliability of the self-calibration function. In summary, the FD-DAS has simple system construction, easy signal processing and other advantages over the methods like DOAS.

Limitations still exist in this study. As shown in the inset of Fig. 1 (b) carefully, minor odd harmonics $3f, 5f, 7f \cdots$ exist in the Fourier spectrum. The reasons are analyzed as: (i) The absorption independent $1f$ sinewave generates a series of harmonics due to the nonlinearity of laser output. (ii) The wavelength ν_0 fails to be located at the accurate center of absorption line shape so that the amplitudes of odd harmonics are not zero. (iii) The residual amplitude modulation (RAM) of laser diode gives rise to the 1st harmonic (1f) of absorption dependent signal p_3. The above three issues will affect the recovered absorption profile. On the other hand, the $1f$ signal from absorption dependent harmonics would mix into the $1f$ absorption independent baseline, as a result weakening the performance of self-calibration function. Fortunately, the trace residual of odd harmonics due to the above three reasons have a minor influence on the FD-DAS results, which has been verified in the experiment section. The response time of FD-DAS has not been optimized in detail because it has something to do with many factors, for example the sinewave scanning frequency, the rate of A/D collection (ADC), the computing capability. Of course, lower sinewave scanning frequency, high-speed ADC and processor prefer to reduce the response time of the FD-DAS method. In our experimental system, a 250 kHz ADC is used to collect the original signal and a laptop is used to process the data. If 128 sinewave cycles of data is employed to perform the FD-DAS, then response time of approximately 1.5 s is achieved.

Approaches can be adopted to deal with the limitations to improve this study. Wavelength calibration has not been involved in this work limited by our current experimental conditions. If an etalon was possible [24] or a k-space sampling clock was built [26], then the nonlinearity of laser wavelength response can be calibrated in the wavelength domain instead of the time domain. Then, the results of absorption profile recovery in Section 4.1 would be enhanced. Furthermore, it would allow us to fix the ν_0 at the absorption center precisely, reducing the influence from absorption-induced odd harmonics as mentioned in (ii). Meanwhile, the Voigt fitting would be conducted in the wavelength

domain instead of the time domain. As a result, the self-calibration performance would be further improved as well. To further improve the response time parameter, the most effective way is to reduce the number of sinewave cycles for Fourier transform. Based on our analysis of existing data, the response time could be improved to ~ 0.6 s if the cycle number was reduced to 60 from 128.

6. Conclusion

Compared to the conventional DAS systems utilizing triangular or sawtooth wave to modulate the laser source, it has certain advantages using sinewave instead. In this study, we proposed a novel Fourier-domain-based method, with just two filters, to successfully recover the intensity scanning baseline and the absorption profile at the same time. The theoretical principle was provided and verified by experiments in a methane detection system. The new FD-DAS method achieved a better result both on Voigt fitting and SNR compared with the DOAS structure under the same conditions. In addition, the separated intensity scanning baseline was used to calibrate the influence of laser power fluctuations. In short, the FD-DAS system is very simple and ultra-easy to implement, and the signal demodulation can be realized by hardware or software. Approaches are still shared in the end to further improve the robustness of the FD-DAS method.

Funding

National Natural Science Foundation of China (52001295, 41575023, U2006209), Natural Science Foundation of Shandong Province (ZR2020QF097, ZR2021QD140), Open Fund of State Key Laboratory of Applied Optics (SKLAO2021001A12), Key Research and Development Program of Shandong Province (2020CXGC010706), Key project of major subject of new and old kinetic energy conversion in Shandong Province (2020XJDN010039), Fundamental Research Funds for the Central Universities (202013024, 202065004), Shandong Postdoctoral Innovation Program, National Key Research and Development Program of China (2019YFC1408301, 2018YFF01011003).

CRediT authorship contribution statement

Rui Liang: Methodology, Software, Validation, Investigation, Visualization. **Fupeng Wang:** Conceptualization, Formal analysis, Writing – original draft. **Qingsheng Xue:** Supervision. **Qiang Wang:** Funding acquisition. **Jinghua Wu:** Resources, Data curation. **Yaopeng Cheng:** Writing – review & editing. **Qian Li:** Project administration.

Declaration of Competing Interest

The authors declare that they have no known competing financial interests or personal relationships that could have appeared to influence the work reported in this paper.

References

[1] P. Puligundla, J. Jung, S. Ko, Carbon dioxide sensors for intelligent food packaging applications, Food Control 25 (1) (2012) 328–333.
[2] M.E. Webber, J. Wang, S.T. Sanders, D.S. Baer, R.K. Hanson, In situ combustion measurements of CO, CO_2, H_2O and temperature using diode laser absorption sensors, Proc. Combust. Inst. 28 (1) (2000) 407–413.
[3] G. Wysocki, Y. Bakhirkin, S. So, F.K. Tittel, C.J. Hill, R.Q. Yang, M.P. Fraser, Dual interband cascade laser based trace-gas sensor for environmental monitoring, Appl. Opt. 46 (33) (2007) 8202–8210.
[4] M. Righettoni, A. Amann, S.E. Pratsinis, Breath analysis by nanostructured metal oxides as chemo-resistive gas sensors, Mater. Today. 18 (3) (2015) 163–171.
[5] C. Wen, X. Huang, C. Shen, Multiple-pass enhanced Raman spectroscopy for fast industrial trace gas detection and process control, J. Raman Spectrosc. 51 (5) (2020) 781–787.
[6] E.D. Hinkley, High–resolution infrared spectroscopy with a tunable diode laser, Appl. Phys. Lett. 16 (9) (1970) 351–354.
[7] M. Loewenstein, Diode laser harmonic spectroscopy applied to in situ measurements of atmospheric trace molecules, J. Quant. Spectrosc. Radiat. Transfer 40 (3) (1988) 249–256.
[8] J. Reid, B.K. Garside, J. Shewchun, M. El-Sherbiny, E.A. Ballik, High sensitivity point monitoring of atmospheric gases employing tunable diode lasers, Appl. Opt. 17 (11) (1978) 1806–1810.
[9] M. Horstjann, Y.A. Bakhirkin, A.A. Kosterev, R.F. Curl, F.K. Tittel, C.M. Wong, C.J. Hill, R.Q. Yang, Formaldehyde sensor using interband cascade laser based quartz-enhanced photoacoustic spectroscopy, Appl. Phys. B 79 (7) (2004) 799–803.
[10] R. Lewicki, G. Wysocki, A.A. Kosterev, F.K. Tittel, QEPAS based detection of broadband absorbing molecules using a widely tunable, cw quantum cascade laser at 8.4 μm, Opt. Exp. 15 (12) (2007) 7357–7366.
[11] V. Spagnolo, P. Patimisco, S. Borri, G. Scamarcio, B.E. Bernacki, J. Kriesel, Part-per-trillion level SF6 detection using a quartz enhanced photoacoustic spectroscopy-based sensor with single-mode fiber-coupled quantum cascade laser excitation, Opt. Lett. 37 (21) (2012) 4461–4463.
[12] L. Dong, R. Lewicki, K. Liu, P.R. Buerki, M.J. Weida, F.K. Tittel, Ultra-sensitive carbon monoxide detection by using EC-QCL based quartz-enhanced photoacoustic spectroscopy, Appl. Phys. B 107 (2) (2012) 275–283.
[13] Q. Ren, C. Chen, Y. Wang, C. Li, Y. Wang, A Prototype of ppbv-Level Midinfrared CO_2 Sensor for Potential Application in Deep-Sea Natural Gas Hydrate Exploration, IEEE Trans. Instrum. Meas. 69 (9) (2020) 7200–7208.
[14] L. Dong, C. Li, N.P. Sanchez, A.K. Gluszek, R.J. Griffin, F.K. Tittel, Compact CH_4 sensor system based on a continuous-wave, low power consumption, room temperature interband cascade laser, Appl. Phys. Lett. 108 (2016) 011106.
[15] R. Cui, L. Dong, H. Wu, S. Li, L. Zhang, W. Ma, W. Yin, L. Xiao, S. Jia, F.K. Tittel, Highly sensitive and selective CO sensor using a 2.33 μm diode laser and wavelength modulation spectroscopy, Opt. Express 26 (19) (2018) 24318–24328.
[16] X. Yin, L. Dong, H. Wu, H. Zheng, W. Ma, L. Zhang, W. Yin, S. Jia, F.K. Tittel, Sub-ppb nitrogen dioxide detection with a large linear dynamic range by use of a differential photoacoustic cell and a 3.5W blue multimode diode laser, Sens. Actuators, B 247 (2017) 329–335.
[17] Y. Ma, Y. Hong, S. Qiao, Z. Lang, X. Liu, H-shaped acoustic micro-resonator-based quartz-enhanced photoacoustic spectroscopy, Opt. Lett. 47 (3) (2022) 601, https://doi.org/10.1364/OL.449822.
[18] C. Yao, S. Gao, Y. Wang, W. Jin, W. Ren, Heterodyne interferometric photothermal spectroscopy for gas detection in a hollow-core fiber, Sens. Actuators, B 346 (2021) 130528.
[19] X. Liu, S. Qiao, Y. Ma, Highly sensitive methane detection based on light-induced thermoelastic spectroscopy with a 2.33 μm diode laser and adaptive Savitzky-Golay filtering, Opt. Express 30 (2) (2022) 1304, https://doi.org/10.1364/OE.446294.
[20] X. Liu, Y. Ma, Sensitive carbon monoxide detection based on light-induced thermoelastic spectroscopy with a fiber-coupled multipass cell [Invited], Chin. Opt. Lett. 20 (2022) 031201.
[21] O. Witzel, A. Klein, C. Meffert, S. Wagner, S. Kaiser, C. Schulz, V. Ebert, VCSEL-based, high-speed, in situ TDLAS for in-cylinder water vapor measurements in IC engines, Opt. Express. 21 (17) (2020) 19951–19965.
[22] Y. Xie, J. Chang, X. Chen, J. Sun, Q. Zhang, F. Wang, Z. Zhang, Y. Feng, A DFB-LD internal temperature fluctuation analysis in a TDLAS system for gas detection, IEEE Photonics J. 11 (3) (2019) 1–8.
[23] F. Wang, J. Chang, C. Zhu, Z. Wang, Y. Liu, W. Wei, C. Jia, Y. Wei, H. Jiang, Demodulation algorithm used in single-beam system immune to light power drift, Appl. Opt. 54 (8) (2015) 2032, https://doi.org/10.1364/AO.54.002032.
[24] Y. Du, Z. Peng, Y. Ding, High-accuracy sinewave-scanned direct absorption spectroscopy, Opt. Express 26 (22) (2018) 29550–29560.
[25] F. Wang, J. Chang, Q. Wang, W. Wei, Z. Qin, TDLAS gas sensing system utilizing fiber reflector based round-trip structure: Double absorption path-length, residual amplitude modulation removal, Sens. Actuators, A 259 (2017) 152–159.
[26] J. Xi, L. Huo, J. Li, X. Li, Generic real-time uniform K-space sampling method for high-speed swept-source optical coherence tomography, Opt. Express. 18 (9) (2010) 9511–9517.